

Article

Dynamic Centrifuge Test and Numerical Modelling of the Seismic Response of the Tunnel in Cohesive Soil Foundation

Zhengfa Chen * and Minghui Bian

Department of Civil Engineering, Changzhou University, 21 Middle Gehu Road, Changzhou 213164, China; 19081402680@smail.cczu.edu.cn

* Correspondence: chenzhengfa@cczu.edu.cn

Abstract: Few studies have been published on the dynamic centrifuge model test of cohesive soil under earthquake action. The seismic response of cohesive soil foundation and tunnel was studied by the centrifuge experiment and numerical modelling. Through a comparison of the acceleration results of tunnel and cohesive soil foundation and the pore pressure and displacement of cohesive soil foundation, the influence of tunnel on cohesive soil foundation is discussed. The weak position of the tunnel under earthquake is predicted by effective numerical modelling. The results show that: (1) Under the Parkfield seismic wave, the natural frequency of the cohesive soil foundation with the tunnel is about 0.3 Hz, which is the most clear for the amplification of the low frequency component and the amplification of the seismic acceleration from bottom to top; (2) The acceleration response of the tunnel itself is small, and the effect of seismic wave on the surrounding soil is weakened due to the existence of tunnels; (3) The maximum bending moment and shear force appear at the corner of the rectangular tunnel, and the maximum axial force appears at the top of the rectangular tunnel; (4) The lateral displacement of the surface soil is the largest, and the pore pressure reduction in the middle soil is the largest compared with other soil layers. The existence of tunnels weakens the liquefaction potential of the surrounding soil.

Keywords: cohesive soil foundation; tunnel; earthquake; dynamic centrifuge test; numerical modelling



Citation: Chen, Z.; Bian, M. Dynamic Centrifuge Test and Numerical Modelling of the Seismic Response of the Tunnel in Cohesive Soil Foundation. *Buildings* **2022**, *12*, 337. <https://doi.org/10.3390/buildings12030337>

Academic Editors: Daniele Zulli and Valeria Settini

Received: 26 January 2022

Accepted: 7 March 2022

Published: 10 March 2022

Publisher's Note: MDPI stays neutral with regard to jurisdictional claims in published maps and institutional affiliations.



Copyright: © 2022 by the authors. Licensee MDPI, Basel, Switzerland. This article is an open access article distributed under the terms and conditions of the Creative Commons Attribution (CC BY) license (<https://creativecommons.org/licenses/by/4.0/>).

1. Introduction

Before the year 1995, scholars from all over the world generally believed that underground buildings were buried in the soil, restricted by the surrounding soil, and were safe under earthquake and difficult to destroy. However, with the continuous development and utilization of underground space, large-section and shallow-buried underground structures were increasing. In reality, seismic disasters also show that these structures were vulnerable to seismic damage, such as the 1995 Kobe earthquake, 1999 Chi-Chi earthquake, and 1999 Kocaeli earthquake [1–4]. Scholars in various countries began to pay attention to the seismic research of underground structures. Currently, research methods for seismic problems of underground structures are mainly analytical methods [5–9], numerical modelling [10–14], and model tests [15–19].

Due to the complexity of dynamic interaction between soil and structure, the theoretical analysis method [20–22] inevitably has certain limitations. Therefore, it is necessary to carry out the research on model tests and numerical modelling. In general, seismic response model tests include the shaking table test and centrifuge shaking table test. Commonly, the ordinary shaking table test equipment is used in 1 g of gravity acceleration environment simulation experiments [23–25]. Compared with the shaking table test, the centrifuge shaking table test can accurately simulate the stress field of the prototype to achieve the same stress field of the model and prototype, which is a more accurate method. Ling et al. [26] studied the anti-floating stability of large diameter pipelines buried in shallow saturated soil under earthquake by the centrifuge test. Dan et al. [27] conducted a centrifuge test

on the soil liquefaction of George Massey immersed tunnel in Canada and the resulting floating problem of tunnel structure. Nakajima et al. [28,29] extended the unit rockfall test and slope model rockfall test to the prototype scale through the dynamic centrifuge model test results, thus rationalizing the design of the protective wall. Enomoto et al. [30,31] studied the effect of reinforcement on the seismic performance of embankment on sand and rigid foundation slopes through a series of dynamic centrifuge model tests. Park et al. [32] conducted a 1:15 model test on the star tower, studied the seismic response characteristics of this ancient building, and explored the reasons for its strong seismic capacity. Yang et al. [33] carried out a series of shaking table tests using geotechnical centrifuge to study the influence of pile spacing on the seismic response of pile raft in the soft soil foundation. Xu et al. [34] analyzed the seismic response and failure mechanism of underground frame structure through a series of dynamic centrifuge model tests. In recent years, with the rapid development of computers, there are continually increasing cases of numerical modelling research [35,36].

The influence of underground structure on earthquake soil liquefaction has also been studied. Ouyang et al. [37] studied the dynamic response of the tunnel in the liquefiable foundation soil layer. The results show that the existence of the tunnel will hinder the liquefaction of the soil, and the influence will change with the stiffness of the tunnel. Chen et al. [38] explored the liquefaction characteristics of saturated sand by combining the numerical simulation and shaking table test. In the study by Bao et al. [39], the pore water pressure near the structure was significantly lower than the free field at the same depth. These results suggest that soil–structure interactions may have an impact. Therefore, in this series of studies, the existence of underground structures, such as tunnels, weakens the liquefaction potential of the surrounding soil. Notably, it is very valuable to use the dynamic centrifuge model test to study the corresponding influence law.

Based on the aforementioned studies, it can be hypothesized that the previous centrifuge test studies mostly focused on the dynamic characteristics of soil, and few studies are published on the seismic deformation of the structure, especially the seismic deformation of the rectangular tunnel. Moreover, many studies are carried out on the dynamic response of non-cohesive soil, and few studies are published on the dynamic centrifuge model test of cohesive soil under earthquake action. In fact, it is also very important to study the dynamic centrifuge test of cohesive soil foundation under earthquake action.

In this paper, the process of developing a cohesive soil foundation model box in the centrifuge test is described in detail. The seismic response of cohesive soil foundation and tunnel was studied by the centrifuge experiment and numerical modelling. In addition, the weak parts of the tunnel and the influence of tunnel existence on the seismic response of foundation are studied, which provide reference for the construction and design of specific projects.

2. Centrifuge Test

2.1. Tunnel Model

A large number of investigations have hypothesized that the destructive effect of earthquakes decays rapidly from the surface to the underground. Therefore, earthquakes generally have little effect on deep tunnels. However, they have a serious impact on shallow tunnels, especially in soft strata [40]. As a result, the model selected in this study is based on the rectangular tunnel with a shallow integral lining structure as the prototype.

For the tunnel structure, the bending capacity and bending strain play a controlling role in safety. Therefore, the model similarity should be based on the bending stiffness. The tunnel is regarded as an elastic rectangular shell structure, and the similarity ratio is derived by the control equation of thin plate bending. The thickness and stress similarity are shown in Equations (1) and (2) by derivation.

$$h_m = \frac{h_p}{n} \left[\frac{E_p}{E_m} \frac{(1 - \mu_m^2)}{(1 - \mu_p^2)} \right]^{\frac{1}{3}} \quad (1)$$

$$\sigma_p = \frac{1 - \mu_p^2}{1 - \mu_m^2} \left(\frac{nh_m}{h_p} \right)^2 \sigma_m \quad (2)$$

In the formula, h_m is the thickness of model lining, h_p is the thickness of prototype lining, σ_p is the bending stress of prototype, σ_m is the bending stress of model lining, the subscripts m and p represent the model and prototype, respectively.

According to the aforementioned equation, the model size can be determined when the centrifuge acceleration is $n = 50$ g. The external size of the model structure can be as follows: $L_m = L_p/n = 5000/20 = 100$ mm; $H_m = H_p/n = 5150/50 = 103$ mm. The elastic modulus and Poisson's ratio of the reinforced concrete structure of the tunnel prototype are as follows: $E_p = 35$ GPa, $\mu_m = 0.17$. The elastic modulus and Poisson's ratio of aluminum alloy for the tunnel model are as follows: $E_p = 70$ GPa, $\mu_m = 0.33$. According to Equation (1), the thickness of the model is $h_m = 4.63$ mm. The structure and size of the prototype and model of the tunnel are shown in Figure 1.

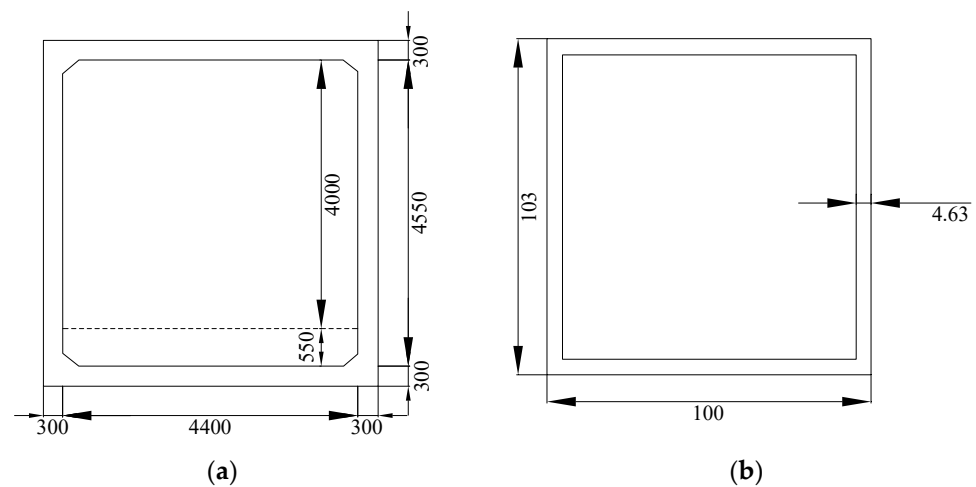


Figure 1. Dimensions of the tunnel: (a) Prototype (unit: mm); (b) Model (unit: mm).

2.2. Preparation of Cohesive Soil Samples

The soil samples used in the test were taken from a site near Beijing Sanyuan Bridge. The maximum dry density of soil $\rho_{dmax} = 1.65$ g/cm³, the optimum moisture content $w_{op} = 21\%$, the plasticity index $I_p = 16.3$, and the specific gravity of soil particle $G_s = 2.72$ were determined according to the Standard for Soil Test Method of China (GB/T 50123-2019, 2019). Following the repeated comparison of several tests, the mud with 50% water content was finally used for sample preparation. Several tests were carried out to compare the fluidity and viscosity of soil samples at various water contents. The fluidity ensures that the soil sample has a higher saturation, and the viscosity allows for the sensors in the soil to be better positioned during shaking. During the preparation, it will be difficult to remove air from soils with lower water content. In addition, air will have a great impact on the data measurement of the test and the saturation of the soil. Soils with high moisture content can result in a difficult tunnel and sensor fixation. Moreover, it is easy to cause the sensor and tunnel to sink during the vibration process, resulting in the failure of the test.

The procedure of the preparation of soil samples for centrifuge testing follows these steps: The first is measuring the water content. The clay soil to be prepared is placed in the indoor crushing and dried. Then, the water content is measured when it remains basically unchanged. The second step is soaking. The soil sample is left to soak by immersion in a mud mixer, according to the specified water content of soil sample preparation. The third step is suction mixing. Here, the soil is first left to soak for 2 days. Then, it is placed in a clay vacuum mixer for suction mixing. When the vacuum reaches the required degree, the soil with uniform mixing is the required clay sample.

The saturated clay sample preparation is presented using the self-developed “saturated clay vacuum mixer” stirring uniform. The procedure of the preparation of soil samples is

as follows: (1) Measuring the water content. The clay soil to be prepared is placed in the indoor crushing, dried, and when the water content is basically unchanged, it is measured, (2) Wetting soil. Soil samples are prepared according to the water content of $w = 50\%$, and the prepared soil samples are immersed in a slurry mixer. The quality of added water in soil is calculated according to Equation (3), (3) Stirring for exhaust. The soil is left to soak for 2 days and then placed in the developed clay vacuum mixer for suction stirring. When the vacuum degree reaches the requirement, the soil with uniform stirring is the required clay sample.

$$\frac{m_T \times \frac{w_T}{1+w_T} + m_w}{m_T \times \left(1 - \frac{w_T}{1+w_T}\right)} = 50\% \quad (3)$$

where m_T represents the quality of soil, w_T represents the water content in soil, and m_w represents the quality of water to be added.

2.3. Model Device

The test adopts a laminated model box ($500 \text{ mm} \times 200 \text{ mm} \times 300 \text{ mm}$). Before loading the soil samples into the model box, a saturated coarse sand layer with a thickness of 8 mm and a particle size of 3–5 mm was placed at the bottom of the model box, and a fine geotextile layer with a thickness of 2 mm was placed on the coarse sand layer. To ensure that the coarse sand layer achieves the purpose of drainage, a hard plastic pipe with an outer diameter of 4.5 mm and an inner diameter of 3 mm was placed in the coarse sand. A small hole with a diameter of 2 mm was punched every 3 cm on the plastic pipe section buried in the coarse sand. The other end of the plastic pipe was extended from the corner of the model box to the upper surface of the soil sample model. To date, the drainage layer under the cohesive soil foundation model is completely established, and the thickness of the drainage layer is about 10 mm. Two accelerometers and one pore pressure sensor were placed in parallel on the upper surface of the drainage layer, and then the uniformly stirred saturated clay sample was placed in the model box. Two rows of accelerometers and two pore pressure sensors were placed in parallel in the middle of the ground model, and two accelerometers were placed on the upper surface of the model. Three displacement sensors were placed on the outside of the model box according to the upper, middle, and lower positions. A layer of 2 mm thick geotextile was placed on the top of the model for use as a drainage layer. At the top and bottom of the tunnel model, a top-out one-way acceleration sensor was placed, and at one side of the model, a side-out one-way acceleration sensor was also placed (see Figure 2 for the sensors and tunnel model layout in model box).

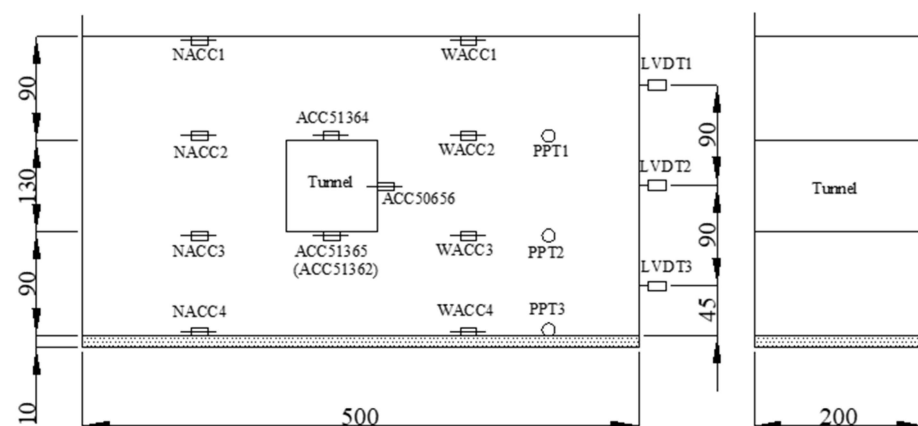


Figure 2. Clay ground model with a tunnel and layout of sensors (unit: mm).

The main acceleration sensors are arranged as follows. NACC refers to the accelerometers on the left, WACC refers to the accelerometers on the right, ACC51364 is the accelerometer at the tunnel top, ACC50656 is the accelerometer at the tunnel side, ACC51365 is the

accelerometer at the bottom of the tunnel, and ACC51362 is the accelerometer near the bottom of the tunnel. In addition, LVDT refers to the linear variable differential transducer arranged on the side of the model box and PPT refers to the pore pressure transducer.

Following the completion of the assembly of model sample, the sample was consolidated. First, under the condition of 1 g, the model is pre-consolidated with 2 kPa. After the ground model has a certain strength, the air extraction consolidation can be carried out. The air extraction consolidation can ensure that not only the pore gas, which is generated in the sample preparation process of the ground model, discharges well. More importantly, the air extraction consolidation can ensure that the consolidation conditions of the ground model reach the same level as the prototype ground when the centrifuge acceleration is $n = 50$ g. The moisture content after the air extraction consolidation is 24%, which is measured by the sampling drying method. This is close to the soil moisture content near Sanyuan Bridge in Beijing.

The following calculation method is used to calculate the negative pressure of pumping. According to the physical parameters of soil samples, the gravity is $\gamma' = 7.3 \text{ kN/m}^3$. Under the condition of 50 g centrifuge acceleration, the gravity of the cohesive soil foundation model is $\gamma'' = n \times \gamma' = 365 \text{ kN/m}^3$, and the stress at the bottom of the ground model is $\sigma' = \gamma'' \cdot h = 98.6 \text{ kPa}$. When the air extraction consolidation is conducted, it is assumed that the required pressure is M when the stress condition in the ground model reaches 50 g, the corresponding water head height is x , and the seepage force acting on the soil is $j = i \times \gamma_w = \gamma_w x / h$. Then, the seepage consolidation stress of negative pressure, which is formed by the air extraction consolidation in soil, is $\sigma' = j \times h = \gamma_w \times x$. Therefore, $x = 9.86 \text{ m}$ can be obtained. As a result, corresponding to the water head $x = 9.86 \text{ m}$, the pressure $M = 98.6 \text{ kPa}$ and the negative pressure is the vacuum degree required for air extraction consolidation. The entire consolidation process lasts for 5 days.

2.4. Application of Seismic Loading

The test was carried out in the 50 g centrifuge acceleration environment created by the centrifuge, and the composition and working principle of the centrifuge shaking table system are shown in Figure 3. Seismic excitation uses the peaking Parkfield seismic wave curve. The acceleration time history curve of the earthquake that occurred in California on 27 June 1966 is shown in Figure 4.

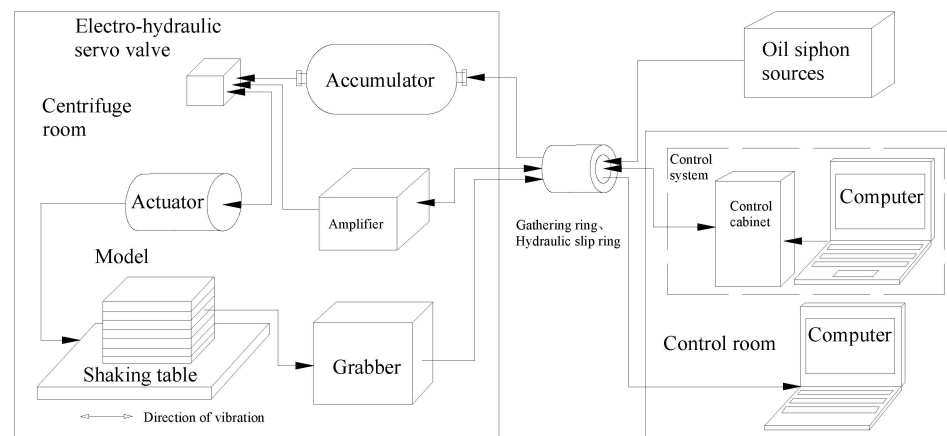


Figure 3. Schematic diagram of vibration table system composition and working principle.

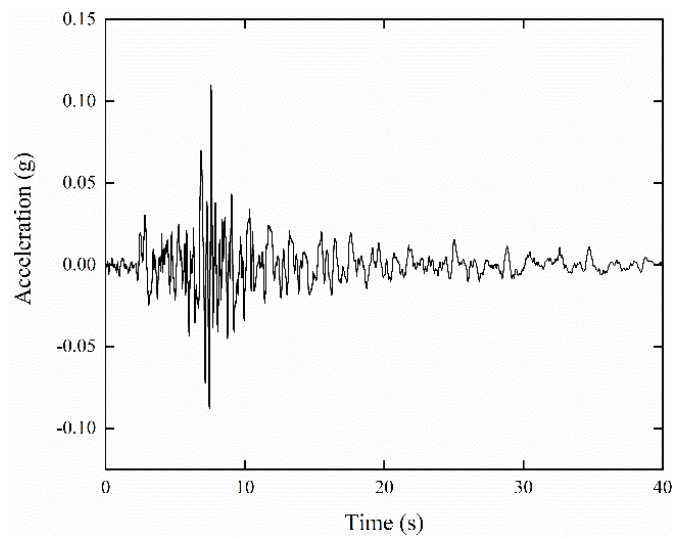


Figure 4. Parkfield seismic wave.

3. Numerical Modelling

3.1. Numerical Model

The data source for model establishment is the prototype corresponding to the model box. The size and thickness of the tunnel are the same as the prototype tunnel. To better compare the centrifuge model test, the tunnel shape is the same as the centrifuge test [41]. Considering the influence of boundary conditions on tunnel modelling, the soil size around the tunnel should be 3–5 times the tunnel diameter. The size of the overlying soil layer on the tunnel model is 12.5 m, the transverse width of the model is 30 m, the vertical bottom of the tunnel is 12.5 m, and the longitudinal length of the tunnel is 30 m, according to the proportion of model tests. The size of the soil outside the tunnel is 25 m, which is 5 times the length of the side of the tunnel. This size is sufficient. The length of the prototype tunnel is 30 m, the height and width are 5 m, and the thickness is 0.3 m. Mesh convergence analysis was performed and the mesh size has little influence on the numerical simulation results. The tunnel was modelled using beam elements, while the soil was meshed by solid elements. The cohesive soil was taken from Sanyuanqiao in Beijing and the related parameters were obtained through laboratory tests. In numerical simulation, cohesive soil is defined by the Mohr–Coulomb constitutive model, and the tunnel is defined by the plastic damage constitutive model. Table 1 shows the material parameters of ground and tunnel.

Table 1. Model parameters.

Model Parameters	Cohesive Soil	Concrete
Poisson's ratio	0.33	0.17
Friction angle (°)	19.2	
Cohesion (kPa)	31	
Elastic modulus (kPa)	1×10^5	3.5×10^7
Density (kg/m ³)	0.73	
Poriness	0.4	
Permeability quotient (cm/s)	1×10^{-7}	

3.2. Boundary Conditions

In previous studies, shell elements were used to simulate the boundary conditions of soil containers [42,43]. As a more suitable boundary condition, the free field boundary has been widely used in simulation [44]. The free field boundary is used to simulate the infiniteness of soil, which is equivalent to fixing the soil from an infinite distance. In addition, it can absorb all of the incident and reflected waves, which is suitable for

seismic dynamic response analysis. Baziar et al. [45] summarized different lateral boundary conditions in numerical modelling to simulate the lateral boundaries of a soil container. In this study, the setting of model boundary conditions is as follows: The base boundary of the model was constrained in both the x-direction and y-direction, the surrounding is set as a free field boundary, and the upper is a free surface. The seismic load is applied from the bottom of the model. Before the time history analysis of the numerical model, the eigenvalue analysis is required to understand the natural vibration characteristics of the structure. Then, the Parkfield seismic wave is applied to the model, and the direct integration method is used to analyze the time history of the numerical model. Figure 5 shows the numerical tunnel model.

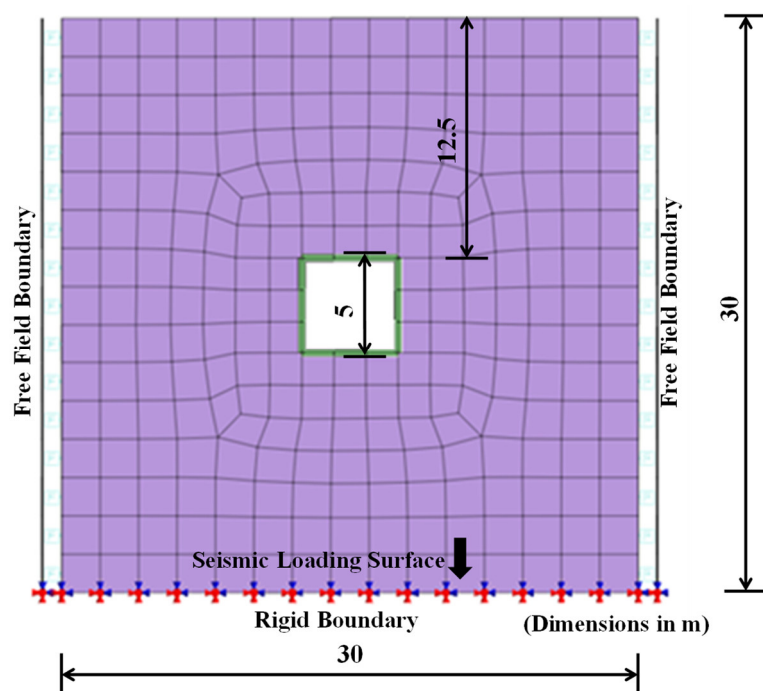


Figure 5. Established numerical tunnel model.

4. Results and Analysis

4.1. Acceleration Response

4.1.1. Acceleration Response of Cohesive Soil Foundation

Figure 6 shows the acceleration response spectrum curve. The NACC in Figure 6 refers to the sensor on the left side of the model box. The sensors are arranged from top to bottom, according to the size of the number. NACC1 is the sensor on the foundation surface, and NACC4 is the sensor on the bottom of the foundation. In Figure 6a, the maximum value of NACC1 is 0.78 g and the maximum value of NACC4 is 0.55 g. It can be seen that the maximum peak acceleration on the surface is significantly higher than the soil bottom. The maximum peak acceleration gradually decreases with the increase in soil depth. The same rule can be found by comparing four acceleration response spectrum curves of numerical modelling, as shown in Figure 6b. With the increase in soil layer thickness, the maximum peak acceleration of seismic wave has a trend of amplification from bottom to top in the viscous soil ground.

The test results and simulation results in Figure 6 both show that the soil has high acceleration response in the low frequency region, which is less than 5 Hz. In particular, this is noticeable in the low frequency region before the peak acceleration is reached. The reason for the greater destructive effect of low frequency seismic waves is revealed.

Figure 7 illustrates the amplification coefficient of acceleration response spectra of the NACC4 and NACC1. The amplification factor corresponding to 0.3 Hz frequency is the largest. It indicates that the natural frequency of the cohesive soil layer in the test under

the Parkfield seismic wave is 0.3 Hz. The cohesive soil foundation has an amplification effect on the low frequency components, especially for the frequency components less than 1.0 Hz, and little amplification effect on the frequency components greater than 10.0 Hz.

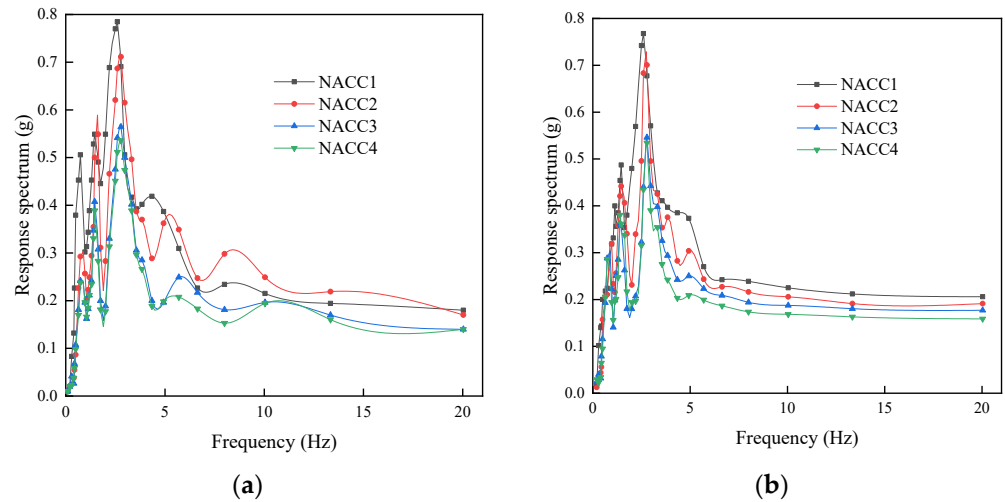


Figure 6. Acceleration response spectra of the cohesive soil foundation: (a) Centrifuge test; (b) Numerical modelling.

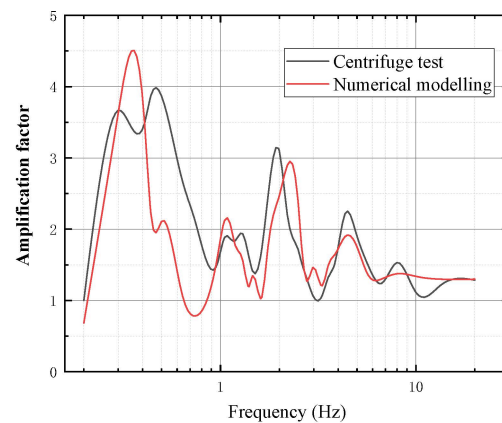


Figure 7. Amplification coefficient of acceleration response spectra (NACC1/NACC4).

4.1.2. Acceleration Response of the Tunnel

Figure 8 shows the acceleration response spectra of the tunnel. In general, the maximum peak acceleration of the acceleration response spectrum curves at the top of the tunnel is the same as the bottom. The maximum peak acceleration of the tunnel sidewall is also the same. This indicates that the vibration amplitude of the tunnel structure itself from bottom to top is the same. The seismic response acceleration on the tunnel is small. The seismic response acceleration on the tunnel is small compared with the cohesive soil foundation.

Figure 9 shows the amplification coefficient of acceleration response spectra of the tunnel, which is from the value of ACC51365 and ACC51364. The amplification coefficients are about 1.0, which indicate that the seismic wave response on the whole tunnel has changed only a little.

4.1.3. Influence of Tunnel on Cohesive Soil Foundation

Figure 10 shows three acceleration response spectrum curves, according to the distance from the tunnel. NACC3 refers to the acceleration response spectrum of soil far from the tunnel. ACC51362 is an acceleration sensor at the same height as NACC3, and is closer to the tunnel. Its acceleration amplitude is between NACC3 and tunnel. This also indicates

that the acceleration amplitude of the earthquake is between the vibration amplitude of the tunnel structure and the vibration amplitude of the free field.

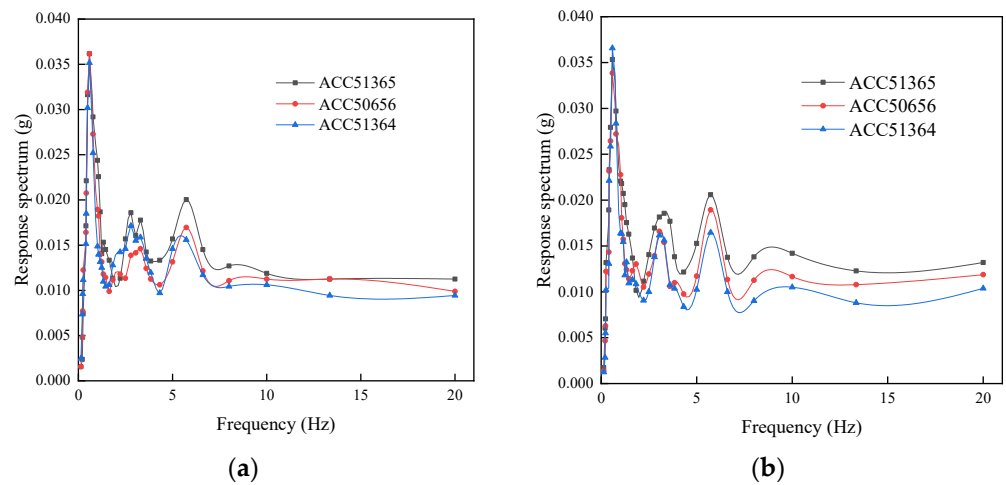


Figure 8. Acceleration response spectra of the tunnel: (a) Centrifuge test; (b) Numerical modelling.

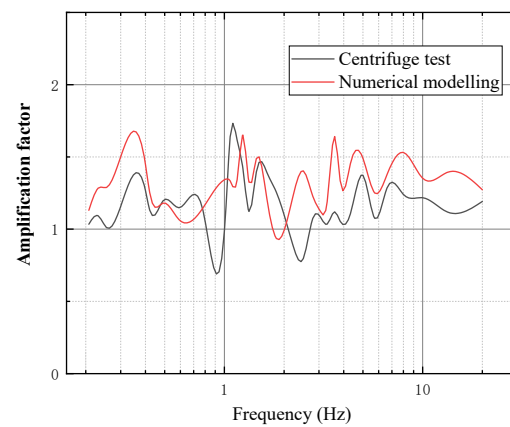


Figure 9. Amplification coefficient of acceleration response spectra (ACC51365/ACC51364).

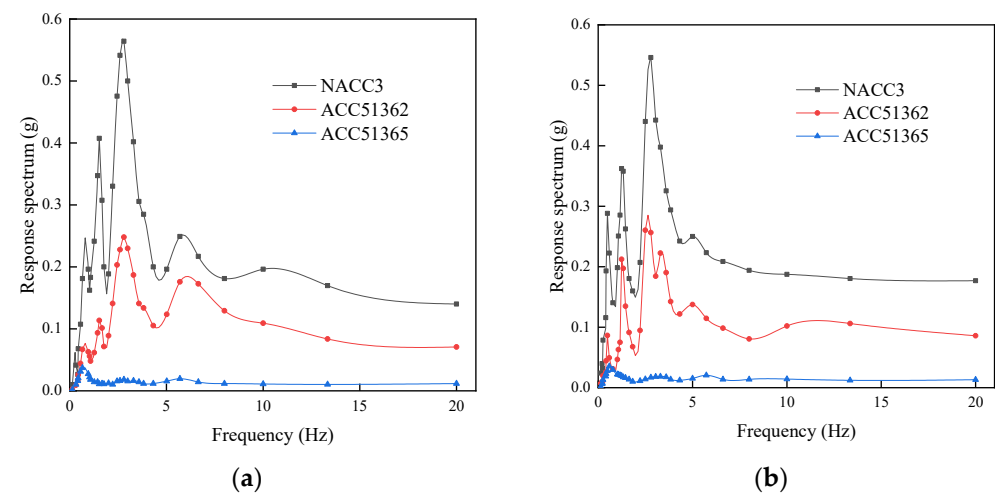


Figure 10. Acceleration response spectra of the soil: (a) Centrifuge test; (b) Numerical modelling.

Compared with the cohesive soil foundation, the seismic response acceleration on the tunnel is small. Therefore, Figure 11 only compares the values of NACC3 and ACC51362. It can be hypothesized that the amplification coefficient of acceleration response spectrum is

up to 5–6 times. This shows that the soil near the tunnel is affected by the tunnel structure, and the existence of tunnel weakens the effect of seismic wave on the surrounding soil.

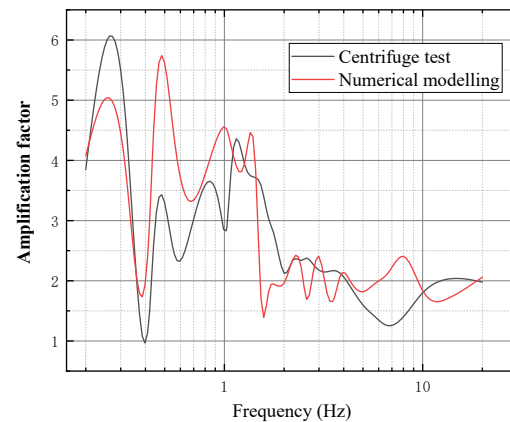


Figure 11. Amplification coefficient of acceleration response spectra (NACC3/ACC51362).

4.2. Internal Force Prediction of the Tunnel

The comparison between the acceleration response spectrum of centrifuge test and numerical modelling are shown in Figure 12. The centrifuge test and numerical simulation, as two means of exploring earthquake action, can not only verify each other, but also complement each other. The errors between the numerical simulation and the experimental results are mostly between 0.8 and 1.2 [46], and it can be seen that the simulation effect is better. In particular, the data in section 0.1–0.3 g are relatively dense, indicating that the numerical simulation and centrifuge test results in the corresponding section are highly consistent. Some of the values exceed the ratio of 0.8, indicating that at the same frequency, the acceleration response value of the centrifuge test is greater than the numerical simulation response value, and there may be certain errors in the test process. This shows that the numerical simulation has good predictive performance, and the possible damage to the tunnel can be judged by numerical simulation.

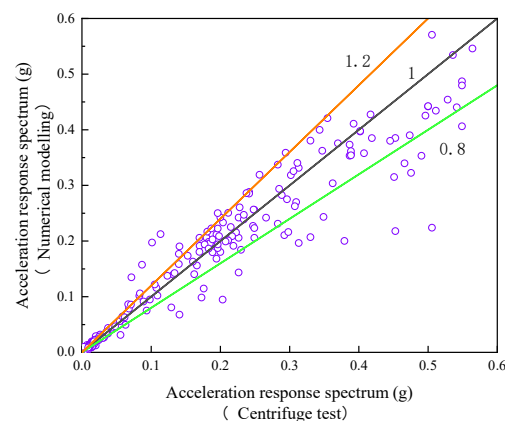


Figure 12. Comparison of acceleration response spectrum from the centrifuge test and numerical modelling.

Figure 13 shows the maximum internal force diagram of the tunnel during the application of y-direction seismic wave, including the bending moment diagram, shear force diagram, and axial force diagram. It can be seen from the shear diagram and bending moment diagram that the maximum shear force and bending moment are located at the corners of the rectangular tunnel. It can also be known from Liu's dynamic centrifuge test that the weak parts of the earthquake are located at four corners of the tunnel section, whether shallow or deep buried tunnels. Therefore, the armpit treatment of rectangular tunnel corners can be considered to improve the seismic capacity of rectangular tunnels.

It can be seen from the axial force diagram that the maximum axial force appears at the top and bottom center of the rectangular tunnel. The axial force at both ends is smaller than the center, which is due to the bearing force of the vertical structure of the rectangular tunnel. Therefore, in the design of rectangular tunnel structure, further reinforcement can be carried out for the weak position in the earthquake.

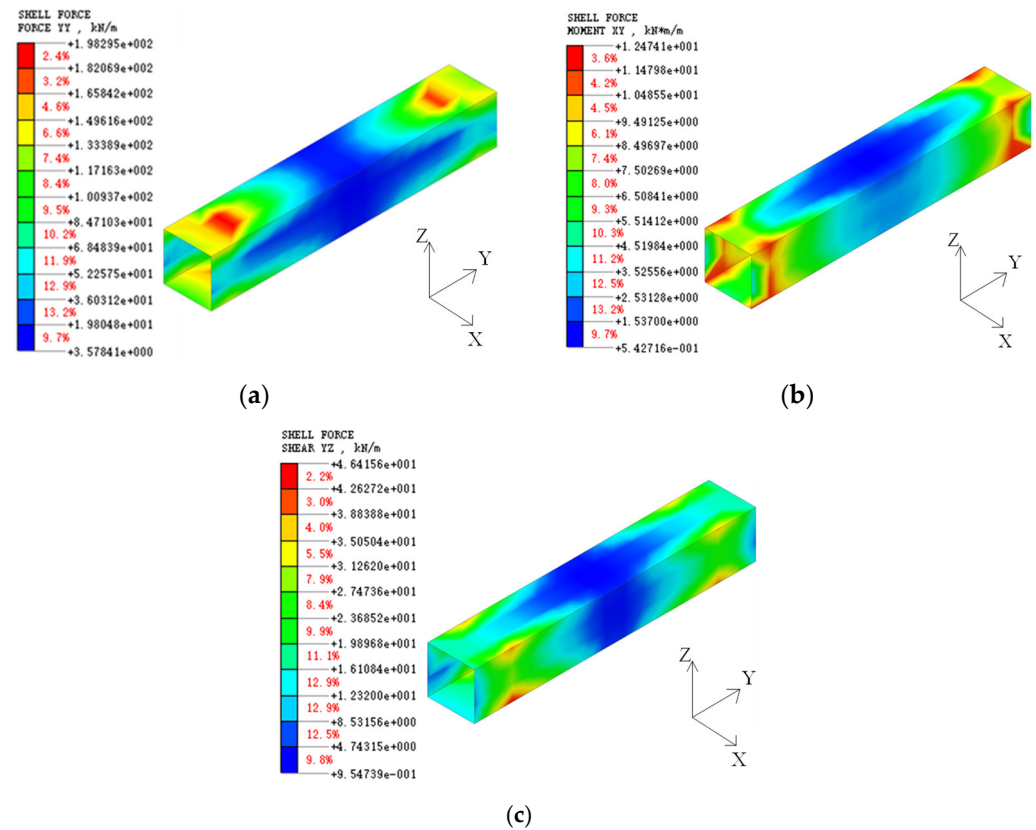


Figure 13. Internal force nephogram of the tunnel: (a) Axial force diagram; (b) Bending moment diagram; (c) Shear force diagram.

4.3. Displacement and Pore Pressure

Figure 14 shows the measurement results of three linear variable differential transducers. LVDT1, LVDT2, and LVDT3 are the lateral displacement of the upper, middle, and lower parts of cohesive soil foundation, respectively. Evidently, the displacement of the upper soil is significantly greater than the other soil layers. The maximum displacement occurs at around 30 s, and is clearly lagging behind the time of peak acceleration of earthquake. Moreover, this illustrates the principle that the earthquake has a great destructive effect on the surface of buildings.

Figure 15 shows the variation in pore pressure. It can be seen that the pore pressure change in the middle soil layer is the largest, and the pore pressure changes in the upper soil layer and the bottom of the soil layer are small. However, the changes in the three pore pressures are the largest at 10 s, and they are all lagging behind the maximum peak acceleration of seismic waves. At the same time, the initial value of pore pressure also increases from top to bottom. When the total stress does not change, the increase in pore pressure will lead to the decrease in effective stress. The change in pore water pressure of the middle layer is larger than the other two layers of soil at around 6 s, and a large reduction value can be identified. Therefore, the effective stress increases and the liquefaction potential of the soil is weakened, which demonstrates that the existence of tunnels weakens the liquefaction potential of the surrounding soil.

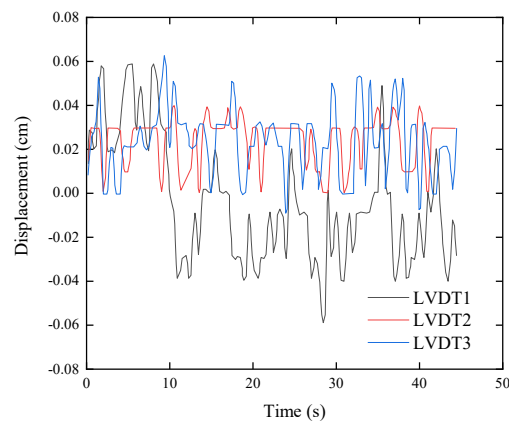


Figure 14. Curves of displacement change.

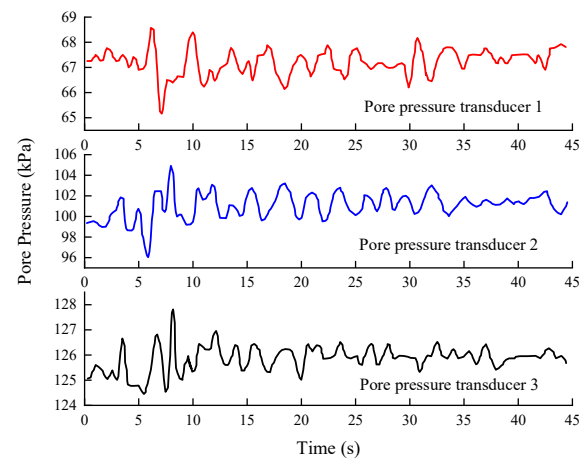


Figure 15. Curve of pore pressure change.

5. Conclusions

This paper describes the process of developing a cohesive soil foundation model box in the centrifuge test in detail. The seismic performance of the tunnel and cohesive soil foundation are investigated using dynamic centrifuge tests and numerical modelling. Through the acceleration response, the weakening effect of the tunnel on the surrounding soil is analyzed. The variation of pore pressure and displacement of clay soil foundation is analyzed, and the possible damage of the tunnel is predicted. The conclusions are summarized as follows:

- (1) The cohesive soil foundation has an amplification effect on low frequency components, especially for the frequency components less than 1.0 Hz. In addition, there is almost no amplification effect on the frequency components greater than 10.0 Hz. Under the Parkfield seismic wave, the natural frequency of viscous soil ground is about 0.3 Hz, which can amplify the seismic acceleration from bottom to top.
- (2) The acceleration response of the tunnel is small, but the acceleration amplitude of the soil near the tunnel is between the vibration amplitude of the tunnel structure and the vibration amplitude of the free field due to the influence of the tunnel structure. The effect of seismic waves on the surrounding soil is weakened, which can be attributed to the existence of tunnels.
- (3) The shear force, bending moment, and axial force diagrams of the rectangular tunnel are obtained by numerical modelling. The maximum bending moment and axial force appear at the corner of the rectangular tunnel, and the axial force appears at the top of the rectangular tunnel. Therefore, in the design of seismic structure, it can be considered to add armpits in the four corners of rectangular tunnel, and strengthen

the construction design of the weak positions, which can effectively improve the seismic effect.

- (4) Regarding the studied cohesive soil foundation with tunnel, a large lateral displacement occurred in the surface soil and a little lateral displacement occurred in the soil below the surface soil during the earthquake. Moreover, the initial pore pressure increases from top to bottom. The pore pressure reduction in the middle soil is the largest compared with the other soil layers. The existence of tunnels weakens the liquefaction potential of the surrounding soil.

Author Contributions: Conceptualization, Z.C.; formal analysis, Z.C.; investigation, Z.C.; resources, Z.C.; data curation, Z.C.; writing—original draft preparation, M.B.; writing—review and editing, M.B.; visualization, Z.C.; supervision, Z.C.; project administration, Z.C.; funding acquisition, Z.C. All authors have read and agreed to the published version of the manuscript.

Funding: This research was funded by the National Natural Science Foundation of China: Thermal–Water–Steam–Mechanical Coupling Characteristics of Saturated Soft Clay under Fire and Its Influence on Tunnel Structure Safety (grant number 51478345).

Conflicts of Interest: The authors declare no conflict of interest.

References

- Hamada, M.; Isoyama, R.; Wakamatsu, K. Liquefaction-induced ground displacement and its related damage to lifeline facilities. *Soils Found.* **1996**, *36*, 81–97. [\[CrossRef\]](#)
- Chou, H.S.; Yang, C.Y.; Hsieh, B.J.; Chang, S.S. A study of liquefaction related damages on shield tunnels. *Tunn. Undergr. Space Technol.* **2001**, *16*, 185–193. [\[CrossRef\]](#)
- Wang, W.; Wang, T.; Su, J.; Lin, C.; Seng, C.; Huang, T. Assessment of damage in mountain tunnels due to the Taiwan Chi-Chi Earthquake. *Tunn. Undergr. Space Technol.* **2001**, *16*, 133–150. [\[CrossRef\]](#)
- Dashti, S.; Hashash, Y.; Gillis, K.; Musgrove, M.; Walker, M. Development of dynamic centrifuge models of underground structures near tall buildings. *Soil Dyn. Earthq. Eng.* **2016**, *86*, 89–105. [\[CrossRef\]](#)
- Wang, J.N. *Seismic Design of Tunnels: A Simple State-of-the-Art Design Approach*; Parsons Brinckerhoff Inc.: New York, NY, USA, 1993.
- Hashash, Y.M.; Hook, J.J.; Schmidt, B.; Yao, J.I.-C. Seismic design and analysis of underground structures. *Tunn. Undergr. Space Technol.* **2001**, *16*, 247–293. [\[CrossRef\]](#)
- Hashash, Y.M.; Park, D.; Yao, J.I.-C. Ovaling deformations of circular tunnels under seismic loading, an update on seismic design and analysis of underground structures. *Tunn. Undergr. Space Technol.* **2005**, *20*, 435–441. [\[CrossRef\]](#)
- Huo, H.; Bobet, A.; Fernández, G.; Ramírez, J. Load transfer mechanisms between underground structure and surrounding ground: Evaluation of the failure of the Daikai Station. *J. Geotech. Geoenviron. Eng.* **2005**, *131*, 1522–1533. [\[CrossRef\]](#)
- Bobet, A.; Fernandez, G.; Huo, H.; Ramirez, J. A practical iterative procedure to estimate seismic-induced deformations of shallow rectangular structures. *Can. Geotech. J.* **2008**, *45*, 923–938. [\[CrossRef\]](#)
- Anastasopoulos, I.; Gerolymos, N.; Drosos, V.; Georgarakos, T.; Kourkoulis, R.; Gazetas, G. Behaviour of deep immersed tunnel under combined normal fault rupture deformation and subsequent seismic shaking. *Bull. Earthq. Eng.* **2008**, *6*, 213–239. [\[CrossRef\]](#)
- Kontoe, S.; Zdravković, L.; Potts, D.; Menkiti, C. On the relative merits of simple and advanced constitutive models in dynamic analysis of tunnels. *Géotechnique* **2011**, *61*, 815–829. [\[CrossRef\]](#)
- Bilotta, E.; Lanzano, G.; Madabhushi, S.P.G.; Silvestri, F. A numerical Round Robin on tunnels under seismic actions. *Acta Geotech.* **2014**, *9*, 563–579. [\[CrossRef\]](#)
- Tsinidis, G. Response characteristics of rectangular tunnels in soft soil subjected to transversal ground shaking. *Tunn. Undergr. Space Technol.* **2017**, *62*, 1–22. [\[CrossRef\]](#)
- Patil, M.; Choudhury, D.; Ranjith, P.; Zhao, J. Behavior of shallow tunnel in soft soil under seismic conditions. *Tunn. Undergr. Space Technol.* **2018**, *82*, 30–38. [\[CrossRef\]](#)
- Cilingir, U.; Madabhushi, S.P.G. Effect of depth on seismic response of circular tunnels. *Can. Geotech. J.* **2011**, *48*, 117–127. [\[CrossRef\]](#)
- Cilingir, U.; Madabhushi, S.P.G. Effect of depth on the seismic response of square tunnels. *Soils Found.* **2011**, *51*, 449–457. [\[CrossRef\]](#)
- Lanzano, G.; Bilotta, E.; Russo, G.; Silvestri, F.; Madabhushi, S.P.G. Centrifuge modeling of seismic loading on tunnels in sand. *Geotech. Test. J.* **2012**, *35*, 854–869. [\[CrossRef\]](#)
- Tsinidis, G.; Ptilakis, K.; Madabhushi, G.; Heron, C. Dynamic response of flexible square tunnels: Centrifuge testing and validation of existing design methodologies. *Geotechnique* **2015**, *65*, 401–417. [\[CrossRef\]](#)
- Moghadam, M.R.; Baziar, M.H. Seismic ground motion amplification pattern induced by a subway tunnel: Shaking table testing and numerical simulation. *Soil Dyn. Earthq. Eng.* **2016**, *83*, 81–97. [\[CrossRef\]](#)
- Penzien, J.; Wu, C.L. Stresses in linings of bored tunnels. *Earthq. Eng. Struct. Dyn.* **2015**, *27*, 283–300. [\[CrossRef\]](#)

21. Penzien, J. Seismically induced racking of tunnel linings. *Earthq. Eng. Struct. Dyn.* **2000**, *29*, 683–691. [[CrossRef](#)]
22. Huo, H.; Bobet, A.; Fernández, G.; Ramírez, J. Analytical solution for deep rectangular structures subjected to far-field shear stresses. *Tunn. Undergr. Space Technol.* **2006**, *21*, 613–625. [[CrossRef](#)]
23. Khan, F.Z.; Ahmad, M.E.; Ahmad, N. Shake table testing of confined adobe masonry structures. *Earthq. Struct.* **2021**, *20*, 149–160. [[CrossRef](#)]
24. Rossi, M.; Calderini, C.; Roselli, I.; Mongelli, M.; de Canio, G.; Lagomarsino, S. Seismic analysis of a masonry cross vault through shaking table tests: The case study of the Dey Mosque in Algiers. *Earthq. Struct.* **2020**, *18*, 57–72. [[CrossRef](#)]
25. Rizwan, M.; Ahmad, N.; Khan, A.N. Seismic performance of RC frame having low strength concrete: Experimental and numerical studies. *Earthq. Struct.* **2019**, *17*, 75–89. [[CrossRef](#)]
26. Ling, H.I.; Mohri, Y.; Kawabata, T.; Liu, H.; Burke, C.; Sun, L. Centrifugal Modeling of Seismic Behavior of Large-Diameter Pipe in Liquefiable Soil. *J. Geotech. Geoenviron. Eng.* **2003**, *129*, 1092–1101. [[CrossRef](#)]
27. Yang, D.; Naesgaard, E.; Byrne, P.M.; Adalier, K.; Abdoun, T. Numerical model verification and calibration of George Massey Tunnel using centrifuge models. *Can. Geotech. J.* **2004**, *41*, 921–942. [[CrossRef](#)]
28. Nakajima, S.; Abe, K.; Shinoda, M.; Nakamura, S.; Nakamura, H.; Chigira, K. Dynamic centrifuge model tests and material point method analysis of the impact force of a sliding soil mass caused by earthquake-induced slope failure. *Soils Found.* **2019**, *59*, 1813–1829. [[CrossRef](#)]
29. Nakajima, S.; Abe, K.; Shinoda, M.; Nakamura, S.; Nakamura, H. Experimental study on impact force due to collision of rockfall and sliding soil mass caused by seismic slope failure. *Landslides* **2020**, *18*, 195–216. [[CrossRef](#)]
30. Enomoto, T.; Sasaki, T. Seismic behaviour of reinforced embankments in dynamic centrifuge model tests. *Soils Grounds* **2018**, *58*, 212–227. [[CrossRef](#)]
31. Enomoto, T.; Sasaki, T. Several factors affecting seismic behaviour of embankments in dynamic centrifuge model tests. *Soils Grounds* **2015**, *55*, 813–828. [[CrossRef](#)]
32. Park, H.-J.; Kim, D.-S. Evaluation of seismic behaviour of Cheomseongdae using dynamic centrifuge model test. *Earthq. Eng. Struct. Dyn.* **2015**, *44*, 695–711. [[CrossRef](#)]
33. Yang, J.; Yang, M.; Chen, H. Influence of pile spacing on seismic response of piled raft in soft clay: Centrifuge modeling. *Earthq. Eng. Eng. Vib.* **2019**, *18*, 719–733. [[CrossRef](#)]
34. Xu, C.; Zhang, Z.; Li, Y.; Du, X. Validation of a numerical model based on dynamic centrifuge tests and studies on the earthquake damage mechanism of underground frame structures. *Tunn. Undergr. Space Technol.* **2020**, *104*, 103538. [[CrossRef](#)]
35. Liu, X.; Chen, H.; Liu, K.; He, C. Model test and stress distribution law of unsymmetrical loading tunnel in bedding rock mass. *Arab. J. Geosci.* **2017**, *10*, 184. [[CrossRef](#)]
36. Polycarpou, P.C.; Petros, K. Numerical investigation of potential mitigation measures for poundings of seismically isolated buildings. *Earthq. Struct.* **2011**, *2*, 1–24. [[CrossRef](#)]
37. Ouyang, Z.; Cui, J.; Li, Y.; Yuan, D. Shaking table test research on tunnel structures with different stiffness in liquefied soil layer. *Mod. Tunn. Technol.* **2018**, *55*, 10.
38. Chen, S.; Tang, B.; Zhuang, H.; Wang, J.; Li, X.; Zhao, K. Experimental investigation of the seismic response of shallow-buried subway station in liquefied soil. *Soil Dyn. Earthq. Eng.* **2020**, *136*, 106153.
39. Bao, X.; Xia, Z.; Ye, G.; Fu, Y.; Su, D. Numerical analysis on the seismic behavior of a large metro subway tunnel in liquefiable ground. *Tunn. Undergr. Space Technol.* **2017**, *66*, 91–106. [[CrossRef](#)]
40. Liu, H.; Huang, M. Centrifugal shaking table test of seismic response of rectangular tunnels with different depths. *Rock Mech. Eng.* **2013**, *2013*, 3404–3412. [[CrossRef](#)]
41. Zhou, H.; Xu, H.; Yang, P.; Zheng, G.; Liu, X.; Zhang, W.; Zhao, J.; Yu, X. Centrifuge and numerical modelling of the seismic response of tunnels in two-layered soils. *Tunn. Undergr. Space Technol.* **2021**, *113*, 103980. [[CrossRef](#)]
42. Chen, J.; Jiang, L.; Li, J.; Shi, X. Numerical simulation of shaking table test on utility tunnel under non-uniform earthquake excitation. *Tunn. Undergr. Space Technol.* **2012**, *30*, 205–216. [[CrossRef](#)]
43. Baziar, M.H.; Moghadam, M.R.; Choo, Y.W.; Kim, D.-S. Tunnel flexibility effect on the ground surface acceleration response. *Earthq. Eng. Eng. Vib.* **2016**, *15*, 457–476. [[CrossRef](#)]
44. Chian, S.C.; Tokimatsu, K.; Madabhushi, S.P.G. Soil liquefaction-induced uplift of underground structures: Physical and numerical modeling. *J. Geotech. Geoenviron. Eng.* **2014**, *140*, 04014057. [[CrossRef](#)]
45. Baziar, M.H.; Moghadam, M.R.; Kim, D.-S.; Choo, Y.W. Effect of underground tunnel on the ground surface acceleration. *Tunn. Undergr. Space Technol.* **2014**, *44*, 10–22. [[CrossRef](#)]
46. Wang, C.; Lai, Y.; Yu, F.; Li, S. Estimating the freezing-thawing hysteresis of chloride saline soils based on the phase transition theory. *Appl. Therm. Eng.* **2018**, *135*, 22–33. [[CrossRef](#)]